Chemical Engineering Journal 165 (2010) 151–160

Contents lists available at ScienceDirect

Chemical Engineering Journal

journal homepage: www.elsevier.com/locate/cej

Experimental design and response surface modeling for optimization of Rhodamine B removal from water by magnetic nanocomposite

Kunwar P. Singh [a,*], Shikha Gupta [a], Arun K. Singh [a], Sarita Sinha [b]

[a] Environmental Chemistry Division, Indian Institute of Toxicology Research, Council of Scientific & Industrial Research, Post Box 80, MG Marg, Lucknow 226 001, UP, India
[b] National Botanical Research Institute, (Council of Scientific & Industrial Research), Rana Pratap Marg, Lucknow 226 001, India

ARTICLE INFO

Article history:
Received 14 July 2010
Received in revised form 4 September 2010
Accepted 6 September 2010

Keywords:
Experimental design
Response surface modeling
Process optimization
Rhodamine dye
Magnetic adsorbent
Nanocomposite

ABSTRACT

A magnetic nanocomposite was developed, characterized, and studied for the removal of Rhodamine B dye from aqueous solution. A four-factor central composite design (CCD) combined with response surface modeling (RSM) and optimization was employed for maximizing the dye removal by the developed nanocomposite based on 30 different experimental data obtained in a batch study. Four independent variables, viz. temperature (10–50 °C), initial pH of solution (2–10), initial dye concentration (140–220 mg/l), and adsorbent dose (1–5 g/l) were transformed to coded values and quadratic model was built to predict the responses. Analysis of variance (ANOVA) and *t*-test statistics were used to test the significance of the independent variables and their interactions. Adequacy of the model was tested by the correlation between experimental and predicted response and enumeration of prediction errors. Optimization of the variables for maximum adsorption of dye by the magnetic nanocomposite was performed using the quadratic model. The predicted maximum adsorption efficiency (47.44 mg/g) under the optimum conditions of the process variables (temperature 50 °C, pH 2, initial dye concentration 220 mg/l, and adsorbent dose 1 g/l) was very close to the experimental value (46.94 mg/g) determined in batch experiment. The Langmuir sorption capacity of the magnetic nanocomposite and its precursor carbon were found to be 33.8 and 4.50 mg/g, respectively (at 50 °C, pH 2, 1 g/l dose, dye concentration 140–220 mg/l), suggesting for the superiority of the developed magnetic adsorbent over its precursor carbon, and for its potential towards removal of the dyes from water/wastewater.

1. Introduction

The synthetic dyes constitute a very important class of water pollutants in view of their large scale production, usage, toxic nature and discharge into surface water bodies along with the industrial wastewater, which leads to water coloration. Rhodamine B (RhB) is a synthetic basic dye imparting red color in aqueous solution. RhB a suspected carcinogen is widely used in paper, textile, leather, and paint industries [1,2]. Due to strong fluorescence produced in aqueous solution, it is employed as the dyeing reagent in the colored glass and characteristic firecrackers [3]. In addition, RhB in combination with auramine-O is also used as a biological stain in many biomedical research laboratories [4]. The basic dyes due to their high tinctorial value are the brightest class of water soluble dyes [5]. Like other synthetic dyes, RhB is also discharged into the surface waters both during its manufacture as well as from the dyeing industries and imparts color undesirable to the water consumers. Human exposure to RhB may cause harmful health effects. It is harmful if swallowed by human beings and animals, and causes irritation to the skin, eyes and respiratory tract [6]. The carcinogenicity, reproductive and developmental toxicity, neurotoxicity and chronic toxicity of RhB towards humans and animals have been reported [7–11].

The color in water bodies reduces penetration of sunlight to the lower layers and hence, affects the aquatic life. Water soluble dyes are characterized by their poor biodegradability and it is estimated that about 20% of the total dye remains in the effluent during the production process [12], thus, building high concentrations in wastewaters. High concentration of the synthetic dyes in the effluents results in the formation of wastewaters characterized by their toxicity, reduced transparency of light and high content of organic load. With the legislations becoming more stringent, considerable importance has been given to the treatment of the dye containing effluents. Consequently, efficient removal and recycling of the dyes in aqueous solution has drawn significant concern. Since, the synthetic dyes are inherently prepared as stable and non-degradable molecules, the conventional treatment methods such as flocculation, chemical or biological oxidation and membrane separation are not suitable for their removal from aqueous phase [12]. Nevertheless, adsorption is shown to be potentially powerful method

* Corresponding author. Tel.: +91 522 2476091; fax: +91 522 2628227.
E-mail address: kpsingh_52@yahoo.com (K.P. Singh).

1385-8947/$ – see front matter © 2010 Elsevier B.V. All rights reserved.
doi:10.1016/j.cej.2010.09.010

for color removal from aqueous phase and a variety of adsorbents derived from various materials have been investigated for their efficiency [13]. However, in view of the large volume of the wastewater with high dye concentration, it is very much desirable to look for some non-toxic low cost efficient adsorbent with the possibility of its regeneration for repeated use. Moreover, in adsorption based technologies, it is very much desirable to have knowledge of the process variables and their influence on adsorption capacity in order to maximize the contaminants removal efficiency of the adsorbents.

Here, we report the results obtained on the preparation of the carbon/iron oxide magnetic nanocomposite from the coconut shell under controlled conditions and its ability to remove RhB from the aqueous phase. Earlier, we have reported efficacy of the activated coconut shell carbons towards the removal of several other molecules from water and wastewater [14–17]. The magnetic adsorbents allow their separation from the liquid phase by simply applying a magnetic field [18]. Magnetized materials have recently been employed for the water purification due to easy control and fast separation [19,20]. The higher adsorption capacity of the magnetic adsorbents for basic cationic dyes has been attributed to the interactions of the hydroxyl groups with the dyes molecules [21]. The liquid–solid interface adsorption process is mainly influenced by the initial concentration of the adsorbate, initial pH of the solution, adsorbent dose, surface area of the adsorbent, contact time, operating temperature and the agitation speed. Optimization of the process conditions is essentially required to maximize the adsorption and hence, the removal efficiency of the adsorbent. The conventional approach for optimization of process variables requires determination of the dependent variable at each and every combination of independent variables just varying only one at a time and keeping all other as constant in batch studies. Such an approach would obviously require a very large number of experiments to be performed, which would be very expensive and time consuming. Moreover, it would not be able to reveal the influence of the interactions between the process variables on the dependent variable [22]. Recently, Singh et al. [23] successfully demonstrated application of the linear and nonlinear modeling approaches, viz. partial least squares (PLS) and artificial neural networks (ANNs) to predict the solid–liquid interface adsorption capacity of activated carbon for the removal of phenol from aqueous solution. However, the study required a large number of batch experiments to be performed. Recently, several types of experimental design methods have been employed in multivariable chemical process optimization. The experimental design method provides statistical models for process variables optimization which help in understanding the interactions among the process variables and their influence on the dependent variable. Another important advantage of the use of statistical models in process optimization is that it requires very less number of experiments to be performed and hence, minimizes time, as well as cost [24]. These techniques involve sound mathematical principles in designing the chemical processes and analyzing the process results. Response surface modeling (RSM) is a useful method for studying the effect of several variables influencing the responses by varying them simultaneously and carrying out a limited number of experiments. A very limited number of studies employing the experimental design and optimization modeling approach for adsorption process have been reported in literature [22–26]. However, there is no information available in literature regarding the optimization of RhB adsorption on magnetic nanocomposites. Therefore, we have undertaken to study the phenomenon of liquid phase adsorption of RhB, in magnetic adsorbent derived from the coconut shell through the experimental design and optimization of the process variables using the response surface modeling approach. The effect of operating variables such as initial concentration of the dye, solution pH, adsorbent dose and operating temperature were optimized.

2. Response surface modeling

RSM is a statistical method that uses quantitative data from appropriate experiments to determine regression model and operating conditions [24]. RSM is basically used for process development and optimization. It helps in evaluating the relative significance of the variables that influence the process. The main objective of RSM is to determine the optimum set of operational variables of the process [27] and is comprised of three basic steps: (a) experimental design; (b) response surface modeling; and (c) process optimization. The statistical experimental designing of an adsorption process can reduce the process variability, experimentation time, overall cost with improved process output [28]. The RSM approach has widely been applied in chemical engineering and sorption process optimization [25].

Central composite design (CCD), a standard RSM design has widely been used for fitting a second-order model and it requires a minimum number of experiments to be performed. For a 2 level study, the total number of experiments to be performed in this type of design are generally given as sum of the 2^n factorial runs, $2n$ axial runs, and n_c center runs ($2^n + 2n + n_c$), where n is the number of independent process variables. The axial points are chosen such that they allow readability, which ensures that variance of the model prediction remains constant at all the points, equidistance from the design center [29]. The replicates at the center provide an independent estimate of the experimental error. In CCD, the factorial or fractional factorial (2^n) levels are coded as ± 1, augmented by the $2n$ axial points ($\pm\alpha$, 0, 0, ..., 0), (0, $\pm\alpha$, 0, ..., 0), (0, 0, ..., $\pm\alpha$), and n_c, the center points (0, 0, 0, ..., 0). The number of center points (replicates) depends on the number of variables considered in the design and is generally between 3 and 10 [27]. The value of α is computed as 1/4th power to the number of factorial runs. Here, for the four variables studied at two levels, $\alpha = (2^4)^{1/4}$. Each variable is investigated at two levels and as the number of variables (n) increases, the number of experimental runs for a complete replicate of the design increases rapidly. In CCD, main effects and interactions between the variables may be estimated by performing a minimum number of experiments.

Once, the experimental design is completed and experimental runs are performed accordingly, the optimization step may be implemented. This involves estimation of the coefficients in a mathematical model and predicting the response and checking the adequacy of the model. The response model may be expressed as:

$$Y = f(X_1, X_2, X_3, \ldots, X_n) \pm e \quad (1)$$

where Y is the response, f is the response function, X_i are the independent variables, and e is the experimental error. The form of response function, f is unknown and may be very complicated. It largely depends on the nature of relationship between the response and the independent variables. RSM aims at approximating f by a suitable polynomial in some region of the independent process variables. A higher order polynomial, such as quadratic model may be expressed as:

$$Y = \beta_0 + \sum_{i=1}^{n} \beta_i X_i + \sum_{i=1}^{n} \beta_{ii} X_1^2 + \sum_{i=1}^{n-1} \sum_{i=1}^{n} \beta_{ij} X_i X_j + e \quad (2)$$

where Y is the predicted response, β_0 the constant coefficient, β_i the linear coefficients, β_{ii} the quadratic coefficients, β_{ij} the interaction coefficients, and X_i, X_j are the coded values of the independent process variables, and e is the residual error.

The RSM helps to investigate the response over the entire variables space and to identify the region where it reaches its optimum

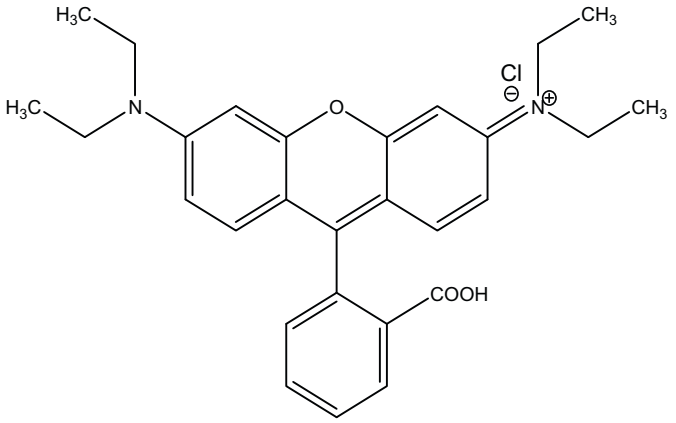

Fig. 1. Chemical structure of Rhodamine B dye in neutral medium.

value. A response surface plot can provide information about the combination of process variables, which gives the best response.

3. Experimental

3.1. Materials

All reagents and chemicals used in the study were of AR grade. Rhodamine B dye (C.I. 45170; $C_{28}H_{31}N_2O_3Cl$; mol. wt. 479; IUPAC name N-[9-(ortho-carboxyphenyl)-6-(diethyl amine)-3H-xanthen-3-ylidene] diethyl ammonium chloride) with the chemical structure (Fig. 1) [30] was procured from M/s Merck, India. The stock solutions of the dye were prepared by dissolving the desired amount of dye in double distilled water. pH of the test solution was adjusted using reagent grade dilute hydrochloric acid and sodium hydroxide.

3.2. Adsorbent development

The adsorption features of the activated carbon and the magnetic properties of iron oxide were combined in a composite to produce magnetic adsorbent. The coconut shell carbon (CSC) was used for preparation of the magnetic nanocomposite. Method for preparation of the CSC is described elsewhere [14]. In brief, the CSC was prepared by treating one part of the coconut shells with two parts (by weight) of concentrated sulfuric acid and the same were kept in an oven maintained at 150–165 °C for a period of 24 h. The carbonized material was washed well with double distilled water to remove the free acid and dried at 105–110 °C for 24 h and subjected to thermal activation at pre-optimized temperature (600 °C) and time (1 h) in an inert atmosphere. The product was then cooled down to the room temperature, sieved (100 mesh size) and stored in a vacuum desiccator until required.

For the preparation of magnetic adsorbent, 10 ml of 10 M sodium hydroxide solution was added drop wise to a suspension of CSC (10 g) in 30 ml aqueous solution of ferric nitrate (10 g) to precipitate the iron oxide. The ratio of the CSC and ferric nitrate in reaction mixture was pre-optimized to achieve optimum magnetic and surface properties of the product. The precipitated material was then agitated at 30 °C for 6 h, filtered and calcinated at 750 °C for 1 h in the presence of nitrogen. The material was then washed thoroughly with double distilled water and dried at 60 °C. The product was sieved to the desired particle size and finally, stored in vacuum desiccators until required [31]. The developed carbon/iron oxide composite was designated as the magnetic nanocomposite.

3.3. Adsorbent characterization

The chemical constituents of the prepared magnetic nanocomposite were determined following the methods reported elsewhere [32,33]. The elemental analysis was performed using the Elemental Analyser model Vario EL-III (Hanau, Germany). The detection limit for C, H, and N were between 0.1 and 1.0 μg. The iron content of the prepared magnetic nanocomposite was determined by atomic absorption spectro-photometry using Perkin Elmer model Analyst-300 model of AAS (USA).

The BET specific surface area (S_{BET}), pore volume (micropore volume, V_{mi}; and total pore volume, V_T), and pore size distribution of the prepared magnetic nanocomposite were determined by N_2-physisorption using the surface area analyzer model Autosorb-1C (Quantachrome, USA). The multipoint Brunauer, Emmett, and Teller (BET) surface area was determined from the nitrogen adsorption/desorption isotherm. The BET isotherm equation is typically applied on the adsorption isotherm in P/P^0 range of 0.05–0.35. Prior to the measurement, the sample was degassed at 100 °C for 8 h in an out-gassing station to remove any adsorbed water or entrapped gases in the sample.

Solid phase analysis was conducted by an X-ray Diffractometer (Panalytical X-pert Pro) at 40 kV and 40 mA. The instrument used copper Kα radiation (λ = 1.54 Å) to produce X-rays with a wavelength of 1.54060 Å. Sample was placed in a zero background metal holder and was scanned from 10–80° 2θ at a rate of 2° 2θ per min. This scan range covered all major species of iron. The mean diameter, d, of the crystallites of the particles was estimated from the pure X-ray diffraction broadening, β, by the Scherrer formula:

$$d = \frac{K\lambda}{\beta \cos\theta}$$

where K is a constant, approximately equal to unity and related to the crystallite shape and to the way in which β and d are defined; λ and θ are the radiation wavelength and Bragg angle, respectively [34].

Scanning electron microscopy (SEM) was used to investigate the surface topography of the developed nanocomposite using the SEM model LEO 430 (Cambridge, England). Samples were set in epoxy and were placed in the sample chamber and evacuated to high vacuum (6.67×10^{-5} Pa). The sample is bombarded with a finely focused electron beam. A three-dimensional topographic image (SEM micrograph) is formed by collecting the secondary electrons generated by the primary beam [14].

The identification of various forms of different constituents in the magnetic nanocomposite was done with the help of IR spectra [17]. The IR spectrum was recorded using the Perkin Elmer FTIR model RX1 (USA) in the range 4000–450 cm^{-1}.

The stability of the prepared magnetic nanocomposite was ensured at extreme acidic pH condition (pH 2) as selected for this study. A known amount of the adsorbent was kept for 24 h in acidic (pH 2) solution. The solution was filtered and iron content was determined in the liquid phase after acid digestion using AAS.

The pH measurements were made using a pH meter (Model 744, Metrohm, Switzerland). Absorbance measurements were made on a Perkin Elmer UV–visible spectrophotometer model Lambada-35. Absorbance values were recorded at the wavelength for maximum absorbance (λ_{max}), i.e. 555 nm for the RhB dye. The concentration of the dye was measured with a 1-cm light-path cell, with an absorbance accuracy of ±0.004 at λ_{max}.

3.4. Process variables and experimental design

The initial concentration of the dye (C_o), initial pH of the solution (pH), adsorbent dose (D), and the operating temperature (T) were identified as the set of four independent process variables to

Table 1
Process control variables and their limits.

Variable	Unit	Notation	Limits				
			−2	−1	0	+1	+2
Temperature	°C	T	10	20	30	40	50
pH	–	pH	2	4	6	8	10
Initial conc. of dye	mg/l	C_o	140	160	180	200	220
Dose	g/l	D	1	2	3	4	5

investigate their influence on the response variable, the removal of the dye from aqueous solution by the prepared magnetic nanocomposite.

The CCD method was adopted to decide the number of the sorption experiments to be performed for optimization of the process variables. For a design of four independent variables ($n = 4$), each with two different levels, the total number of experiments (N) was worked out as; $N = (2^n + 2n + n_c) = 2^4 + (2 \times 4) + 6 = 30$. Here, this includes the standard 2^n factorial points with their origin at the center, $2n$ axial points fixed at a distance, α from the center to generate the quadratic terms, and n_c replicate points at the center [27]. After having defined the range of each of the process variables, they are coded to lie at ±1 for the factorial points, 0 for the center points and $\pm\alpha$ for the axial points. The numerical values of the variables were transformed into their respected coded values as:

$$X_i = \frac{2X - (X_{max} - X_{min})}{X_{max} - X_{min}} \quad (3)$$

where X_i is the required coded value of a variable X. X_{min} and X_{max} are the low and high values of X. The selected process variables with their limits, units and notations are given in Table 1.

3.5. Sorption procedure

Batch experiments were conducted to study the effect of various operating variables on the dye adsorption rate. All the experiments were conducted according to the CCD matrix at random, to avoid the possibility of any systematic errors in measurements. Minimum and maximum levels of each of the four process variables were defined through pre-trial experiments. Stability of the dye (RhB) was ensured at the extremes of the pH and temperature selected for the study. For sorption of the dye on developed magnetic nanocomposite, different weighted amounts of the adsorbent (1–5 g/l) were equilibrated with 50 ml of solution initially containing 140–220 mg/l of the dye. The aqueous solutions of the dye were prepared by dissolving known amount of RhB in 1 l of double distilled water. The working standard solutions of the dye (140–220 mg/l) were prepared by diluting the stock solution and their pH were adjusted (2–10) precisely using dilute hydrochloric acid and sodium hydroxide. The sorption experiments were conducted in a thermo-controlled (±1 °C) water bath shaker for 60 min at 120 rpm at different temperatures (10–50 °C). The contact time and other conditions were selected on the basis of the results obtained for preliminary experiments. The equilibrated samples were taken out and the aqueous solution phase was separated from the adsorbent using a centrifuge to make it carbon free. The residual concentration of the dye in the solution was then determined using the UV–vis spectrophotometer at 555 nm (λ_{max} of the dye). The adsorption (mg/g) of the dye by the adsorbent was calculated as [14];

$$q_e = \frac{(C_o - C_e)V}{W} \quad (4)$$

where C_o and C_e are the initial and final concentrations (mg/l) of the dye in solution, respectively. The V and W represent the solution volume (l) and adsorbent weight (g), respectively. All sorption experiments were performed in duplicate and the mean of the two are taken for all calculations. The experimental conditions and the corresponding dye adsorption (mg/g) measured through the batch experiments are presented in Table 2.

3.6. Response surface modeling

The response variable, Y (adsorption, mg/g) of the dye from the aqueous solution by the developed magnetic carbon can be expressed as; $Y = f(X_T, X_{pH}, X_{Co}, X_D)$, where, X_T, X_{pH}, X_{Co}, and X_D are the coded values of the process variables (operating temperature, initial pH of solution, initial dye concentration, and adsorbent dose) The selected relationship being a second degree response surface expressed as below;

$$Y = \beta_0 + \beta_1 X_T + \beta_2 X_T^2 + \beta_3 X_{pH} + \beta_4 X_{pH}^2 + \beta_5 X_{Co} + \beta_6 X_{Co}^2 + \beta_7 X_D + \beta_8 X_D^2 + \beta_9 X_T X_{pH} + \beta_{10} X_T X_{Co} + \beta_{11} X_T X_D + \beta_{12} X_{pH} X_{Co} + \beta_{13} X_{pH} X_D + \beta_{14} X_{Co} X_D \quad (5)$$

The model coefficients are estimated and used for predicting the response values for different combinations of the coded values of the variables.

The adequacy of the selected model and statistical significance of the regression coefficients were tested using the analysis of variance (ANOVA) and the student's t-test statistics. The measured and model predicted values of the response variable were used to compute the correlation coefficient (R^2), the root mean square error of prediction (RMSEP) and the relative standard error of prediction (RSEP). The correlation between the measured and predicted values indicates the goodness of fit of the model, whereas, the RMSEP and RSEP values are used to evaluate the predictive ability of the selected model. The RMSEP and RSEP were computed as:

$$\text{RMSEP} = \sqrt{\frac{\sum_{i=1}^{N}(y_{pred,i} - y_{meas,i})^2}{N}} \quad (6)$$

$$\text{and} \quad \text{RSEP} = \sqrt{\frac{\sum_{i=1}^{N}(y_{pred,i} - y_{meas,i})^2}{\sum_{i=1}^{N}(y_{meas,i})^2}} \times 100 \quad (7)$$

where $y_{pred,i}$ and $y_{meas,i}$ represent the model predicted and measured values of the dependent variable (adsorption capacity) and N represents the number of experimental observations. The RMSEP and RSEP are measure of the goodness-of-fit, best describes an average measure of the error in predicting the dependent variable by the selected model [35]. The RSM was performed using the Statistica 7.0.

Table 2
Central composite design (CCD) for the four independent variables (coded values) and corresponding dye adsorption (mg/g).

Serial no.	CCD term	No. of experiments	Process variables (coded values)				Adsorption (mg/g)
			T	pH	C_o	D	
1	Factorial (2^n)	16	−1, +1	−1, +1	−1, +1	−1, +1	18.42–32.51
2	Axial ($2n$)	8	−2, 0, +2	−2, 0, +2	−2, 0, +2	−2, 0, +2	18.02–29.48
3	Center (n_c)	6	0	0	0	0	22.18–22.52

3.7. Model validation and process optimization

The model validation was performed through generating several sets of different combinations of the independent process variables (temperature, pH, initial dye concentration, and adsorbent dose) each within their experimental ranges at constant contact time and agitation speed and corresponding response variable (adsorption mg/g) was generated using the model equation after having transformed the process variables into their respective coded values using Eq. (3). Batch experiments were conducted to determine the response variable under fixed conditions of all the process variables for each defined validation set. The model predicted and experimental values of the response variable for validation set were used to compute the correlation coefficient (R^2), the root mean square error of prediction (RMSEP) and the relative error of prediction (RSEP).

The developed quadratic model was used to optimize the process variables within their studied experimental ranges. Optimization was performed in Excel 97.

4. Results and discussion

4.1. Characterization of the adsorbent

The pH of the prepared magnetic adsorbent was measured after stirring 1.0 g of the carbon with deionized water (100 ml, pH 6.8) for 2 h. Its pH was found 7.65. The elemental analysis of the prepared magnetic adsorbent revealed its chemical constituents as: C 54.31%, H 1.97%, and N 0.31%. The atomic absorption spectrophotometric measurement determined the total iron content of the prepared carbon/iron oxide nanocomposite as 9.47%. The result of the stability check of the magnetic adsorbent in acidic medium (pH 2) revealed that about 20% of the total iron content (94.7 mg/g) of the adsorbent dissolved and leached to the acidic solution at pH < 2. The specific surface area of the adsorbent was evaluated from the N_2 isotherms by applying the Brunaeur, Emmett and Teller (BET) equation and was found 335 m^2/g. The S_{BET} area of the magnetized nanocomposite (335 m^2/g) was lower than its normal precursor (CSC) [14]. This decrease in the surface area of the magnetic nanocomposite as compared with its precursor CSC may be attributed to the formation of iron oxide nanoparticles inside the pores. The total and micropore volumes of the adsorbent were determined as 0.234 and 0.198 cm^3/g, respectively, and the average pore diameter was 2.78 nm. Fig. 2 illustrates the X-ray diffractogram (XRD) of the prepared magnetic nanocomposite in the 2θ range of 10–80°. Six narrow peaks at 2θ values of 30.07°, 35.44°, 43.16°, 54.65°, 57.14°, and 62.67° indicate that the adsorbent is crystalline in nature [34]. The calculated crystallite sizes (diameter) computed by the Scherrer's equation were found to be in the range of 10.6–19.80 nm. Since the carbon is amorphous in nature, the observed crystallinity of the magnetic adsorbent originated due to the iron oxide [31]. In the present study, scanning electron microscopic (SEM) photograph of the magnetic adsorbent revealed the surface texture, porosity and fibrous structure of the developed nanocomposite (Fig. 3). The surface micrograph showed a distinct roughness pattern with distinct carbon and iron oxide particles, which appear brighter (Fig. 3a). Fig. 3b shows details of the iron oxide particle in nanocomposite. The coarse and rough morphology of the composite could provide more reactive sites than the smooth morphology, and thereby, was in favour of the sorption of dye from aqueous solution [36]. Different constituents in developed carbon/iron oxide nanocomposite were identified with the help of IR spectra [17]. The IR spectrum of the developed adsorbent (Fig. 4) showed weak and broad peaks in the region of 3874–453 cm^{-1}. Approximate FT-IR band assignment indicated the presence of

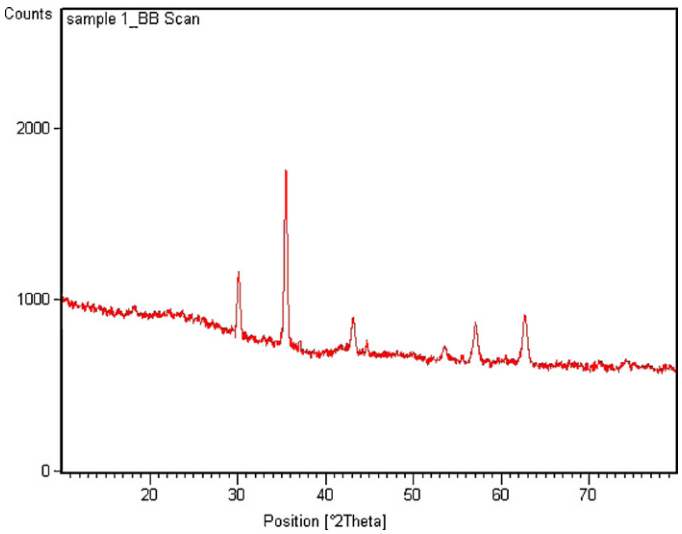

Fig. 2. X-ray diffractogram (XRD) of the prepared magnetic adsorbent.

carbonyl, carboxyls, lactones, phenols, olefinic and aromatic structures. The broad band at 3404.4 cm^{-1} represented –OH group. The 1800–1540 cm^{-1} bands are associated with C=O stretching mode in carbonyls, carboxylic acids, and lactones and C=C bonds in olefinic and aromatic structures, whereas the 1440–1000 cm^{-1} band was assigned to the C–O and O–H bending modes. The assignment of a specific wave number to a given functional group was not possible because the absorption bands of various functional groups overlap and shift, depending on their molecular structure and environment. Shifts in absorption positions can be caused by the factors such

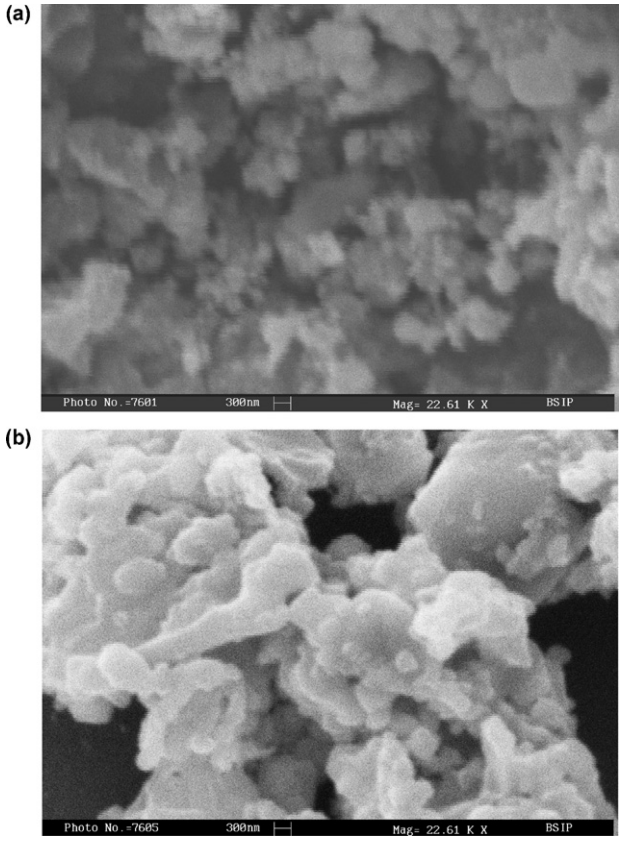

Fig. 3. Scanning electron micrograph (SEM) of (a) activated carbon/iron oxide composite and (b) iron oxide in composite.

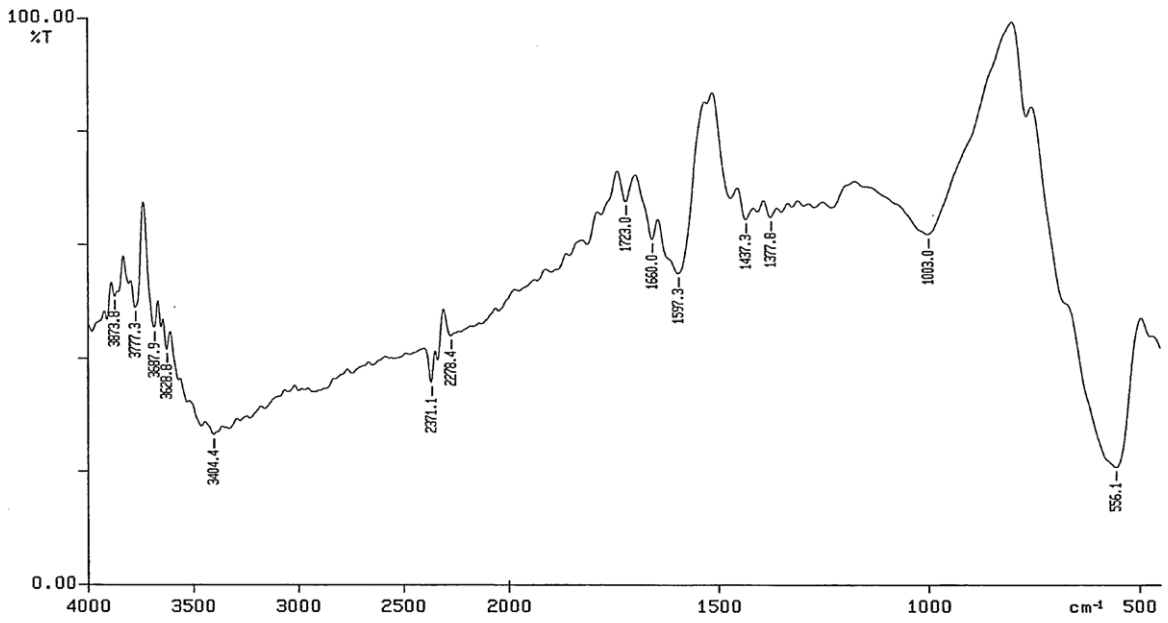

Fig. 4. FTIR spectra of the prepared magnetic adsorbent.

as intra-molecular and intermolecular hydrogen bonding, steric effects, and degrees of conjugation [17].

A contact of the laboratory magnet with the water suspension containing the prepared carbon/iron oxide nanocomposite immediately led to aggregation of all the particles collected on the inner surface of the container near the magnet (Fig. 5) and the clear (particles free) solution could be easily decanted off. This suggests that the prepared nanocomposite possessed magnetism and could be potentially used as a magnetic adsorbent to remove the compounds in liquid phase.

4.2. Response surface modeling

In the present study, the linear, quadratic and interactive influences of the four process variables (viz. temperature, pH, dye concentration, and adsorbent dose) on the adsorption of RhB dye on developed magnetic adsorbent were investigated. The five different levels of the four selected variables are presented in Table 1.

4.2.1. Experimental design and quadratic model

CCD was adopted for studying the adsorption of RhB from the aqueous solution by the magnetic adsorbent. A quadratic model was selected for developing the mathematical relationship between the response and the four operating process variables, viz. initial dye concentration, initial pH of the dye solution, dose of the adsorbent and operating temperature. The CCD helps in designing the experiment to obtain a quadratic model, here consisting of 2^4 standard factorial runs, a star configuration ($\alpha = \pm 2$) of size, $2n$, and six replicates at the center point (n_c) used to determine the experimental error. The maximum adsorption of the dye was observed to be 32.51 mg/g. A polynomial regression modeling was performed between the response variable, Y (adsorption, mg/g) and the corresponding coded values (X_T, X_{pH}, X_{Co}, and X_D) of the four different process variables (T, pH, C_o, D), and finally, the best fitted model equation was obtained as:

$$Y\,(mg/g) = 22.32 + 3.27X_T + 0.42X_T^2 - 1.43X_{pH} + 0.75X_{pH}^2 + 0.10X_{Co} + 0.37X_{Co}^2 - 1.82X_D + 0.47X_D^2 - 0.13X_TX_{pH} + 0.01X_TX_{Co} - 0.48X_TX_D - 0.23X_{pH}X_{Co} + 0.33X_{pH}X_D + 0.23X_{Co}X_D \quad (8)$$

Eq. (8) was used to evaluate the influence of the process variables on the response factor, the dye removal rate (Y) from aqueous solution by the developed magnetic adsorbent. The statistical analysis results (Table 3) are expressed in terms of the degrees of freedom (DF), sum of squares (SS), mean squares (MS), F and p values. The MS value is obtained by dividing the SS value by DF. The computed F-value is the ratio of the MS_{effect} and $MS_{residual}$ values. Thus, the higher the F-value, the greater is the significance of the corresponding variable (term) to cause effect. From the statistical analysis (Table 3), it is evident that all the linear (except dye concentration) and quadratic terms are statistically significant ($p < 0.05$, where p denotes the probability), whereas among the interactive terms the temperature and dose interaction is significant. Almost a similar pattern has been reported by others [22]. The regression coefficients and the ANOVA results (Table 3) further suggested that the temperature (T), the adsorbent dose (D), and the pH are among the parameters exhibiting most significant effect on the adsorption rate. For the regression coefficients, both the magnitude and sign are important, as the earlier indicates the importance or influence of the variable on the response factor, whereas, the sign determines its effect direction. A positive sign of the coefficient represents a synergistic effect, while a negative sign indicates an antagonistic effect. The variables pH and the dose and the interactive term temperature and dose (T^*D) had negative significant relationship with the dye adsorption process, whereas, the interactive terms, temperature and pH (T^*pH) and pH and dye concentration (pH$^*C_o$)

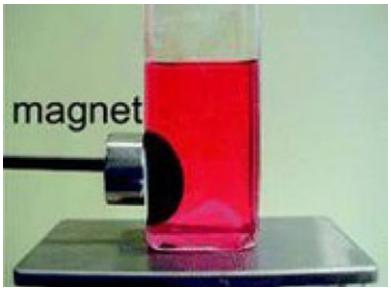

Fig. 5. Separation of magnetic adsorbent particles from the solution by a magnet.

Table 3
The ANOVA results for the response surface quadratic model for adsorption of the RhB dye.

Source	Coefficient	Sum of squares	DF	Mean squares	*F*-value	*p*-Value	Remarks
Intercept	22.32	2989.63	1	2989.63	5213.183	0.000000	Significant
X_T	3.27	257.094	1	257.094	448.309	0.000000	Significant
X_{pH}	−1.43	48.886	1	48.886	85.246	0.000000	Significant
X_{Co}	0.097	0.225	1	0.225	0.392	0.540506	
X_D	−1.82	79.261	1	79.261	138.212	0.000000	Significant
X_T^2	0.42	4.848	1	4.848	8.453	0.010831	Significant*
X_{pH}^2	0.75	15.569	1	15.569	27.148	0.000106	Significant
X_{Co}^2	0.37	3.838	1	3.838	6.692	0.020627	Significant
X_D^2	0.47	6.018	1	6.018	10.494	0.005502	Significant
$X_T^* X_{pH}$	−0.13	0.269	1	0.269	0.469	0.503782	
$X_T^* X_{Co}$	0.007	0.001	1	0.001	0.002	0.969181	
$X_{pH}^* X_{Co}$	−0.23	0.864	1	0.864	1.506	0.238702	
$X_T^* X_D$	−0.48	3.680	1	3.680	6.416	0.022955	Significant
$X_{pH}^* X_D$	0.33	1.771	1	1.771	3.088	0.099256	
$X_{Co}^* X_D$	0.23	0.821	1	0.821	1.432	0.249990	

DF – degrees of freedom.

exhibited having negative but less significant effect on dye adsorption.

The experimentally determined and the model predicted values of the response variable, the adsorption (mg/g) of the dye, are presented in Fig. 6. A fairly high correlation ($R^2 = 0.98$) between the measured and the model predicted values of the response variable and reasonably low RMSEP (0.54) and RSEP (0.41) values suggest for the adequacy of the fitted quadratic model for predictive applications.

4.2.2. Model validation

Validation of the selected quadratic model was performed through generating five sets with different combinations of the independent process variables each within the respective experimental range and corresponding values of the response variable (adsorption, mg/g) were generated using the coded values of the process variables and model equation (8). Experimentally determined response factor values for each of the five set of process variables were then used along with the model predicted values to compute the correlation coefficient, RMSEP and RSEP values. The model predicted and experimental results are presented in Table 4. A high correlation ($R^2 = 0.97$) among the predicted and the measured values of the response factor (Fig. 7) and considerably low RMSEP (0.38) and RSEP (0.69) values suggest for the adequacy of the selected quadratic model in predicting the response variable for the validation data set comprised of different combinations of the process variables.

4.2.3. Dye adsorption capacity of the magnetic adsorbent

The dye adsorption capacity (mg/g) of the prepared magnetic nanocomposite and its precursor CSC were evaluated using the Langmuir sorption isotherm, which is based upon the assumption of monolayer adsorption onto a surface containing finite number of adsorption sites of uniform energies of adsorption with no transmigration of the adsorbate in the pores of the adsorbent surface. The linear form of the Langmuir isotherm may be written as:

$$\frac{C_e}{C_e} = \frac{1}{Q^0 b} + \frac{C_e}{Q^0}$$

where q_e is the amount of solute adsorbed per unit weight of adsorbent (mg/g), C_e the equilibrium concentration (mg/l), Q^0 the monolayer adsorption capacity (mg/g) and b is the constant (l/mg) related to the free energy of adsorption ($b \propto e^{-\Delta G/RT}$). It is the value reciprocal of the concentration at which half the saturation of the adsorbent is attained. The model parameters (Q^0 and b) can be determined from the linear plots of C_e/q_e and C_e [14]. The isotherm (figure not shown due to brevity) showed a good fit to the experimental data ($R^2 = 0.97$). The sorption capacity of the magnetic nanocomposite and its precursor CSC were found to be 33.8 and 4.50 mg/g, respectively, at 50 °C and pH 2. The adsorption capacity values of the two adsorbents suggest for the superiority of the magnetic nanocomposite over the precursor CSC and for its potential towards removal of the dyes from water/wastewater.

The influence of the different process variables on the response factor (adsorption, mg/g) are visualized in the 3D response surface plots (Fig. 8a–f).

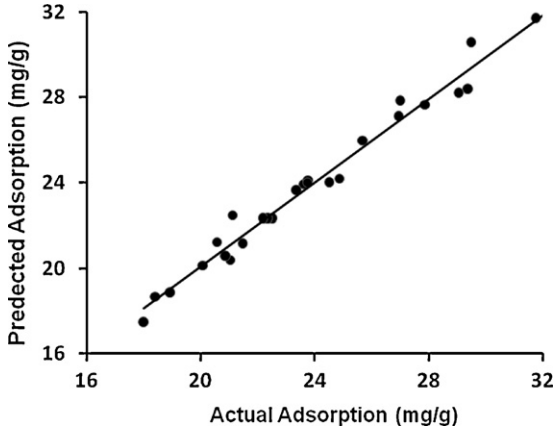

Fig. 6. Plot of the actual and predicted adsorption (mg/g) of the RhB for the model development set.

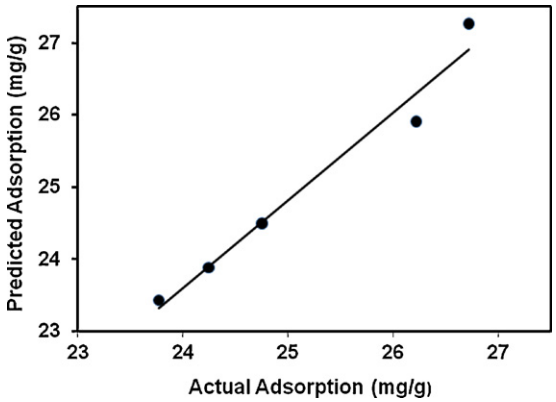

Fig. 7. Plot of the actual and predicted adsorption (mg/g) of the RhB for the model validation set.

Table 4
The actual (*A*) and coded (*C*) values of the independent process variables in model validation set and corresponding values of the response variable.

Experiment no.	Temperature (°C)		pH		Adsorbent dose (g/l)		Initial conc. of dye (mg/l)		Adsorption (mg/g)	
	A	*C*	*A*	*C*	*A*	*C*	*A*	*C*	Pred.	Expt.
1	15	−1.5	3	−1.5	1.5	−1.5	150	0.25	25.72	25.40
2	25	−0.5	5	−0.5	2.5	−0.5	170	0.75	23.27	22.93
3	35	0.5	7	0.5	3.5	0.5	190	1.25	23.75	23.38
4	45	1.5	9	1.5	4.5	1.5	210	1.75	26.22	26.76
5	32	0.2	6	0	3	0	200	1.5	24.26	23.98

Pred – model predicted; Expt – experimental.

4.2.3.1. Effect of temperature and pH. In adsorption processes, both the temperature and solution pH play very important role. These variables are considered to be most effective in influencing the sorption process. Fig. 8a shows the three-dimensional response surfaces representing the combined effect of temperature and pH on adsorption of the dye at constant initial dye concentration (180 mg/l) and adsorbent dose (3 g/l). An increase in the temperature within the experimental range shows an enhancement in the adsorption rate of the dye. A similar trend with temperature has also been reported earlier [37–40]. It may be attributed to either relatively higher affinity of the sites for dye or an increased number of the binding sites in the adsorbent with increase in temperature [22]. Moreover, an increase in temperature would decrease the viscosity of the solution and hence enhances the rate of diffusion of the adsorbate molecules in the internal pores of the adsorbent particles [41]. Further, the figure shows that the rate of the dye adsorption in the experimental pH range 2–10, decreases with increase in pH of the solution. A similar trend has also been reported earlier [38]. The reason for this type of behavior at the adsorbent–dye interface may be due to the nature of the adsorbent acquiring negative charge on the surface, and hence exhibiting high affinity for the cationic dyes (RhB), which are positively charged in acidic medium. In alkaline pH range, the dye (RhB) acquires negative charge, thus resulting into decline of the adsorption capacity of the adsorbent. A maximum adsorption of dye (29.48 mg/g) was determined at constant initial concentration (180 mg/l) and adsorbent dose (3 g/l).

4.2.3.2. Effect of temperature and initial concentration of dye. The interactive effect of process temperature and initial concentration of the dye in solution on the adsorption by the prepared magnetic carbon at constant pH (6.0) and dose (3 g/l) is shown in Fig. 8b. It is evident that adsorption rate in the experimental range increases with increasing temperature. Jain et al. [38] also reported an increase in dye uptake with increasing concentration. However, the uptake rate increases with increasing dye concentration at low temperature, whereas, the trend reversed at higher temperature, exhibiting a decreased uptake with increasing dye concentration. Further, with increasing dye concentration, an increase in the adsorption rate at low temperature may be understood in view of the larger availability of the dye molecules for adsorption. A similar trend has also been observed by other workers [31]. A maximum dye removal (29.48 mg/g) was determined at constant pH (6) and dose (3 g/l).

4.2.3.3. Effect of temperature and adsorbent dose . The combined effect of temperature and adsorbent dose on the dye uptake by the magnetic carbon is shown in Fig. 8c. It may be noted that the adsorption of the dye increases with increase in temperature as earlier. However, a declining trend is noted with increasing dose of the adsorbent in the experimental range. In a solution of constant dye concentration, an increasing dose may lead to declining in the number of dye molecules in solution, hence reduced flux from the solution bulk to the adsorbent surface. A maximum dye removal (29.48 mg/g) was observed at constant pH (6) and dye concentration (180 mg/l).

4.2.3.4. Effect of pH and initial dye concentration. Fig. 8d shows the interactive influence of pH and initial concentration of the dye on adsorption from the aqueous phase. It is evident that the dye uptake increases with increase in the dye concentration and declines with increasing pH of the solution in the experimental range as in cases discussed earlier. Declining trend in dye uptake with increasing pH may be attributed to the similar charges (negative) on adsorbent surface and the dye molecules in the alkaline medium. A maximum dye removal (>29 mg/g) was observed at constant temperature (30 °C) and adsorbent dose (3 g/l).

4.2.3.5. Effect of pH and adsorbent dose. The response surface plot for combined effect of the solution pH and the adsorbent dose (Fig. 8e) suggests that at lower pH, the dye uptake by the magnetic adsorbent increases with the increasing dose, whereas, the trend reverses at higher (alkaline) pH in the experimental range. Such a behavior may be due to the reversal in ionic structure of the dye in acidic and basic medium. The RhB dye molecule acquires a positive charge in acidic pH medium, whereas, a negative charge in alkaline medium. So, despite an increase in number of binding sites with the dose, repulsive forces at the adsorbent–dye interface may lead to a decreased uptake. A maximum dye removal (>29 mg/g) was observed at constant temperature (30 °C) and initial dye concentration (180 mg/l).

4.2.3.6. Effect of initial dye concentration and adsorbent dose. The combined effect of adsorbent dose and initial dye concentration is visible in Fig. 8f. It may be seen that at low doses, the dye uptake decreases with increasing concentration, whereas, at higher doses, the uptake increases with dye concentration. It may be attributed to the fact that for low dose, increasing dye concentration after saturation of the binding sites would result into decline of the uptake, whereas, at higher doses, the uptake would be relatively higher due to availability of relatively more active binding sites. At constant temperature (30 °C) and adsorbent dose (3 g/l), a maximum dye removal of 27 mg/g was determined.

4.2.4. Optimization of the dye adsorption

Optimization of the process variables to maximize the adsorption of the RhB dye by the developed adsorbent from the aqueous solution was performed using the quadratic model within the studied experimental range of various process variables. The process optimization modeling suggested the optimum values of different process variables (viz. temperature 50 °C, pH 2, initial dye concentration 220 mg/l, and adsorbent dose 1 g/l) to achieve the maximum removal (47.44 mg/g) of the RhB dye from the solution in an equilibrium time of 1 h. The corresponding experimental value of the dye adsorption was determined as 46.94 mg/g, which is very close to the optimum value predicted by the model.

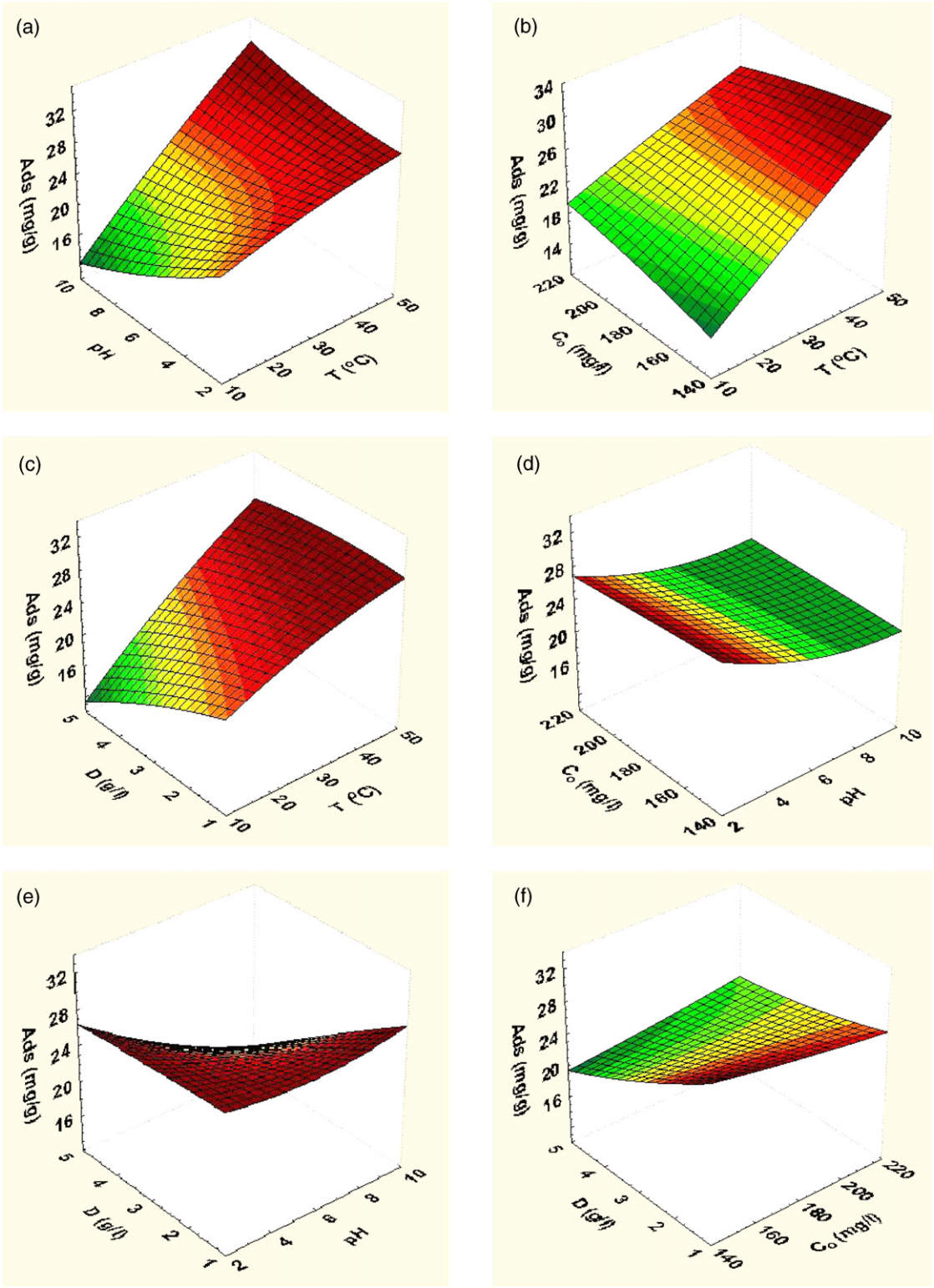

Fig. 8. The 3D plots showing effect of (a) temperature and pH, (b) temperature and initial dye concentration, (c) temperature and adsorbent dose, (d) pH and initial dye concentration, (e) pH and adsorbent dose, and (f) initial dye concentration and adsorbent dose on the adsorption of RhB dye.

5. Conclusions

The present study aimed to develop and determine the adsorption capacity of the magnetic adsorbent (carbon/iron oxide nanocomposite) and to optimize the process variables to maximize the RhB dye removal from the aqueous phase. The RSM based on full factorial CCD was used to determine the effect of four different process variables, viz. temperature, solution pH, initial dye concentration, and adsorbent dose on the dye adsorption capacity of the magnetic adsorbent from the aqueous solution. A second-order quadratic model used for response surface analysis identified the temperature, dose, and pH as the most significant variables influencing the dye adsorption process. The process optimization for maximum removal of the dye identified the process conditions

(temperature 50 °C, pH 2, adsorbent dose 1 g/l, and dye concentration 220 mg/l). The adsorption of dye (mg/g) determined through the batch experiment (46.94 mg/g) was found to agree closely with the model predicted value (47.44 mg/g). The experimental design and RSM approach successfully determined the adsorption capacity of the magnetic adsorbent for RhB dye from the aqueous solution and optimization of process variables for maximum dye removal. Moreover, the dye removal capacity of the developed carbon/iron oxide magnetic nanocomposite was much higher than its precursor CSC and hence, the magnetic adsorbent may be used for removal of the dye from waste/wastewater.

Acknowledgement

The authors thank the Director, Indian Institute of Toxicology Research, Lucknow (India) for his keen interest in the work.

References

[1] Y. Wong, J. Yu, Laccase-catalyzed decolorization of synthetic dyes, Water Res. 33 (1999) 3512–3520.
[2] I.M. Banate, P. Nigam, D. Singh, R. Marchant, Microbial decolorization of textile dye containing effluents: a review, Bioresour. Technol. 58 (1996) 217–227.
[3] J.M. Drake, R.I. Morse, R.N. Steppel, D. Young, Kiton red S and rhodamine B. The spectroscopy and laser performance of red laser dyes, Chem. Phys. Lett. 35 (1975) 181–188.
[4] I. Poulios, A. Avranas, E. Rekliti, A. Zouboulis, Photocatalytic oxidation of Auramine O in the presence of semiconducting oxides, J. Chem. Technol. Biotechnol. 75 (2000) 205–212.
[5] G. McKay, Adsorption of dyestuffs from aqueous solutions with activated carbon. I: Equilibrium and batch contact-time studies, J. Chem. Technol. Biotechnol. 32 (1982) 759–772.
[6] J. Rochat, P. Demenge, J.C. Rerat, Toxicologic study of a fluorescent tracer: rhodamine B, Toxicol. Eur. Res. 1 (1978) 23–26.
[7] D. Kornbrust, T. Barfknecht, Testing of 24 food, drug, cosmetic, and fabric dyes in the in vitro and the in vivo/in vitro rat hepatocyte primary culture/DNA repair assays, Environ. Mutagen. 7 (1985) 101–120.
[8] IARC, Overall evaluation of carcinogenicity: an updating of IARC Monograph (1987) 1–42.
[9] J.C. Mirsalis, C.K. Tyson, K.L. Steinmetz, E.K. Loh, C.M. Hamilton, J.P. Bakke, J.W. Spalding, Measurement of unscheduled DNA synthesis and S-phase synthesis in rodent hepatocytes following in vivo treatment: testing of 24 compounds, Environ. Mol. Mutagens 14 (1989) 155–164.
[10] D.B. McGregor, A.G. Brown, S. Howgate, D. McBride, C. Riach, W.J. Caspary, Responses of the L5178Y mouse Lymphoma cell forward mutation assay. V: 27 Coded chemicals, Environ. Mol. Mutagens 17 (1991) 196–199.
[11] T. Shimada, H. Yamazaki, M. Mimura, Y. Inui, F.P. Guengerich, Interindividual variations in human liver cytochrome P-450 enzymes involved in the oxidation of drugs, carcinogens and toxic chemicals: studies with liver microsomes of 30 Japanese and 30 Caucasians, J. Pharm. Exp. Ther. 270 (1994) 414–423.
[12] J. Huang, K. Huang, S. Liu, A. Wang, C. Yan, Adsorption of Rhodamine B and methyl orange on a hypercrosslinked polymeric adsorbent in aqueous solution, Colloids Surf. A 330 (2008) 55–61.
[13] P.P. Selvam, S. Preethi, P. Basakaralingam, N. Thinakaran, A. Sivasamy, S. Sivanesan, Removal of rhodamine B from aqueous solution adsorption onto sodium montmorillonite, J. Hazard. Mater. 155 (2008) 39–44.
[14] K.P. Singh, A. Malik, S. Sinha, P. Ojha, Liquid-phase adsorption of phenols using activated carbons derived from agricultural waste material, J. Hazard. Mater. 150 (2008) 626–641.
[15] D. Mohan, K.P. Singh, D. Ghosh, Removal of α-Picoline, β-Picoline, and γ-picoline from synthetic wastewater using low cost activated carbons derived from coconut shell fibers, Environ. Sci. Technol. 39 (2005) 5076–5086.
[16] D. Mohan, K.P. Singh, S. Sinha, D. Ghosh, Removal of pyridine derivatives from aqueous solution by activated carbons developed from agricultural waste materials, Carbon 43 (8) (2005) 1680–1693.
[17] D. Mohan, K.P. Singh, S. Sinha, D. Ghosh, Removal of pyridine from aqueous solution using low cost activated carbons derived from agricultural waste materials, Carbon 42 (12–13) (2004) 2409–2421.
[18] M. Schwickardi, S. Olejnik, E.L. Salabas, W. Schmidt, F. Schuth, Scalable synthesis of activated carbon with superparamagnetic Properties, Chem. Commun. (2006) 3987–3989.
[19] C.F. Chang, P.H. Lin, W. Höll, Aluminum-type superparamagnetic adsorbents: synthesis and application on fluoride removal, Colloids Surf. A 280 (2006) 194–202.
[20] S.S. Banerjee, D.H. Chen, Fast removal of copper ions by gum Arabic modified magnetic nano-adsorbent, J. Hazard. Mater. 147 (2007) 792–799.
[21] S. Pirillo, M.L. Ferreira, E.H. Rueda, Adsorption of alizarin, eriochrome blue black R, and fluorescein using different Iron oxides as adsorbents, Indus. Eng. Chem. Res. 46 (2007) 8255–8263.
[22] J.N. Sahu, J. Acharya, B.C. Meikap, Response surface modeling and optimization of chromium(VI) removal from aqueous solution using Tamarind wood activated carbon in batch process, J. Hazard. Mater. 172 (2009) 818–825.
[23] K.P. Singh, P. Ojha, A. Malik, G. Jain, Partial least squares and artificial neural networks modeling for predicting chlorophenol removal from aqueous solution, Chemom. Intell. Lab. Syst. 99 (2009) 150–160.
[24] Z. Alam, S.A. Muyibi, J. Toramae, Statistical optimization of adsorption processes for removal of 2,4-dichlorophenol by activated carbon derived from oil palm empty fruit bunches, J. Environ. Sci. 19 (2007) 674–677.
[25] P. Ricou-Hoeffer, I. Lecuyer, P.L. Cloirec, Experimental design methodology applied to adsorption of metallic ions onto fly ash, Water Res. 35 (2001) 965–976.
[26] U.K. Garg, M.P. Kaur, V.K. Garg, D. Sud, Removal of Nickel(II) from aqueous solution by adsorption on agricultural waste biomass using a response surface methodological approach, Bioresour. Technol. 99 (2008) 1325–1331.
[27] R.H. Myers, D.C. Montgomery, Response Surface Methodology, second ed., Wiley, 2001.
[28] G. Annadurai, R.S. Juang, D.J. Lee, Adsorption of heavy metals from water using banana and orange peels, Water Sci. Technol. 47 (2003) 185–190.
[29] G.E.P. Box, J.S. Hunter, Multifactor experimental design for exploring response surfaces, Ann. Math. Stat. 128 (1957) 195–241.
[30] H.M.H. Gad, A.A. El-Sayed, Activated carbon from agricultural by-products for the removal of Rhodamine-B from aqueous solution, J. Hazard. Mater. 168 (2009) 1070–1081.
[31] R. Ahmad, R. Kumar, kinetics and thermodynamics studies of brilliant green adsorption onto carbon/iron oxide nanocomposite, J. Kor. Chem. Soc. 54 (2010) 125–130.
[32] A.L. Vogel, A Text Book of Quantitative Chemical Analysis, ELBS Publication, London, England, 1991.
[33] G. McKay, Use of Adsorbents for the Removal of Pollutants from Wastewater, CRC Press, Boca Raton, FL, 1995.
[34] F.M. De, Y. Peng, C.T. Hu, H.H. Ping, Y. Aihua, C.K. Min, Z.J. Xi, L. Dong, Synthesis, characterization and size control of zerovalent iron nanoparticles anchored on montmorillonite, Chin. Sci. Bull. 55 (2010) 1092–1099.
[35] K.P. Singh, N. Basant, A. Malik, G. Jain, Modeling the performance of "up-flow anaerobic sludge blanket" reactor based wastewater treatment plant using linear and nonlinear approaches-A case study, Anal. Chim. Acta 658 (2010) 1–11.
[36] W. Xiangyu, C. Chau, C. Ying, L. Huiling, Dechlorination of chlorinated methanes by Pd/Fe bimetallic nanoparticles, J. Hazard. Mater. 161 (2009) 815–823.
[37] Y. Guo, J. Zhao, H. Zhang, S. Yang, J. Qi, Z. Wang, H. Xu, Use of rice husk-based porous carbon for adsorption of Rhodamine B from aqueous solutions, Dyes Pigments 66 (2) (2005) 123–128.
[38] R. Jain, M. Mathur, S. Sikarwar, A. Mittal, Removal of the hazardous dye rhodamine B through photocatalytic and adsorption treatments, J. Environ. Manage. 85 (2007) 956–964.
[39] B.S. Inbaraz, N. Sulochana, Use of jackfruit peel carbon (JPC) for adsorption of rhodamine-B, a basic dye from aqueous solution, Ind. J. Chem. Technol. 13 (2006) 17–23.
[40] Sumanjeet, T.P.S. Walia, I. Kansal, Removal of Rhodamine-B by adsorption on walnut shell charcoal, J. Surf. Sci. Technol. 24 (2008) 179–193.
[41] S. Wang, Z.H. Zhu, Effects of acidic treatment of activated carbons on dye adsorption, Dyes Pigments 75 (2) (2007) 306–314.